Preparation of theophylline inhalable microcomposite particles by wet milling and spray drying: the influence of mannitol as a co-milling agent

Maria Malamatari[1], Satyanarayana Somavarapu[1], Kyriakos Kachrimanis[2], Mark Bloxham[3], Kevin MG Taylor[1], Graham Buckton[1]

[1] *UCL School of Pharmacy, 29-39 Brunswick Square, London, WC1N 1AX, UK*

[2] *Department of Pharmaceutical Technology, Faculty of Pharmacy, Aristotle University of Thessaloniki, 54124 Thessaloniki, Greece*

[3] *GSK Medicines Research Centre, Gunnels Wood Road, Stevenage, Hertfordshire, SG1 2NY, UK*

Corresponding author: Graham Buckton

UCL School of Pharmacy,

29-39 Brunswick Square,

London, WC1N 1AX, UK

Email: g.buckton@ucl.ac.uk

Tel/Fax: +44 (0) 2077535858

ABSTRACT: Inhalable theophylline particles with various amounts of mannitol were prepared by combining wet milling in isopropanol followed by spray drying. The effect of mannitol as a co-milling agent on the micromeritic properties, solid state and aerosol performance of the engineered particles was investigated. Crystal morphology modelling and geometric lattice matching calculations were employed to gain insight into the intermolecular interaction that may influence the mechanical properties of theophylline and mannitol. The addition of mannitol facilitated the size reduction of the needle-like crystals of theophylline and also their assembly in microcomposites by forming a porous structure of mannitol nanocrystals wherein theophylline particles are embedded. The microcomposites were found to be in the same crystalline state as the starting material(s) ensuring their long-term physical stability on storage. Incorporation of mannitol resulted in microcomposite particles with smaller size, more spherical shape and increased porosity. The aerosol performance of the microcomposites was markedly enhanced compared to the spray-dried suspension of theophylline wet milled without mannitol. Overall, wet co-milling with mannitol in an organic solvent followed by spray drying may be used as a formulation approach for producing respirable particles of water-soluble drugs or drugs that are prone to crystal transformation in an aqueous environment (i.e. formation of hydrates).

Keywords: Co-milling, dry powders for inhalation, mannitol, spray drying, theophylline

1. INTRODUCTION

The classical formulation approach for drug delivery to the lungs using dry powder inhalers (DPIs) is micronising the active pharmaceutical ingredient (API) and then mixing with a suitable coarse carrier (e.g. lactose, mannitol). Micronisation (e.g. by ball or air-jet milling for particle size reduction) may generate amorphous domains on the drug particle surface. The amorphous state tends to revert back to a lower energy and more stable crystalline state upon storage, which may adversely influence the product performance as it affects critical particle properties such as the morphology, particle size distribution, dissolution and aerosolisation (Brodka-Pfeiffer et al., 2003; Chow et al., 2007). Therefore, preparation of nanosuspensions by a wet size reduction technique (e.g. wet milling, high pressure homogenisation, antisolvent precipitation) followed by solidification, using spray drying, has been suggested as a preparation platform for inhalable micron-sized composites of nanocrystals with enhanced dissolution and aerosolisation efficiency (Bosch et al., 1999; Malamatari et al., 2015; Pilcer et al., 2009; Yamasaki et al., 2011).

The majority of such reported applications (nanos-in-micros particle engineering approach) has focused on poorly water-soluble drugs and thus the size reduction step can take place in aqueous media where the drug is dispersed but not dissolved (Duret et al., 2012; Pomázi et al., 2013). However, some drugs used for the treatment of respiratory diseases are moderately or very water-soluble, such as salbutamol sulfate (albuterol sulfate) and terbutaline sulfate, or are prone to hydrate formation, e.g. nedocromil sodium. Therefore, water cannot be used as

the wet milling medium, in the preparation of nanosuspensions, nor as the solvent during the spray-drying step as for poorly water-soluble drugs. Instead, an appropriate organic solvent has to be selected, in which the drug exhibits a solubility lower than 10 mg ml^{-1} and ideally lower than 5 mg ml^{-1} (Hong and Oort, 2011), to eliminate the possibility of crystallinity changes (e.g. amorphisation) during milling and spray drying.

Theophylline has been chosen as the model compound in this study as it has a long history of use within respiratory medicine, and its solid-state properties have been extensively investigated. More specifically, anhydrous theophylline is a challenging molecule with respect to wet milling and spray drying due to the following physicochemical properties:

(i) It is a moderately water-soluble drug (7.36 mg ml^{-1}, at 25 ^{o} C, Yalkowsky and He, 2003).

(ii) Its needle-like crystal shape morphology can affect its fracture/breakage behavior, as reported for other organic crystalline materials.

(iii) It is prone to process-induced solid-state transformations as it exists in four polymorphic forms (forms I-IV) along with a monohydrate form (Fucke et al., 2012). Form II is the stable polymorph at room temperature while the monohydrate is the stable form in water and at high relative humidity environment.

From a pharmacological point of view, theophylline is a widely available and inexpensive methylxanthine that has been used in the treatment of

airway diseases such as asthma and chronic obstructive pulmonary disorder (COPD) for more than 90 years (Barnes, 2013).

The use of theophylline has been limited by its narrow therapeutic index (TI) and marked inter-subject variability of its clearance. A therapeutic plasma concentration of 10 - 20 mg L^{-1} is required for theophylline to achieve bronchodilation comparable with β_2-agonists, while side effects (e.g. nausea, vomiting, heartburn, diarrhea) become an issue at concentrations above 20 mg L^{-1} (Barnes, 2013). Due to its narrow TI, it is administered as oral sustained-release (SR) preparations.

There is increasing evidence that theophylline at low doses (plasma concentrations < 7 mg L^{-1}) exhibits immunomodulatory properties in the pathophysiology of both asthma and COPD (Barnes, 2013). Moreover, it has been reported that theophylline has the potential to enhance the anti-inflammatory effect of corticosteroids and reverse steroid resistance that is common in COPD patients (Hirano et al., 2006; Tilley, 2011). These observations may lead to the reevaluation of this old drug in the future, once clinical trials of low-dose theophylline therapy are completed (Barnes, 2008; 2003).

Theophylline applied intratracheally as a dry powder formulation to the airways of anaesthetised guinea pigs exhibited smooth muscle relaxant and anti-inflammatory properties at very low doses that would be predicted to have no systemic toxicity (Raeburn and Woodman, 1994). Thus, developing inhalable formulations for theophylline may offer advantages over oral administration for the treatment of inflammation in asthma and COPD, enhancing the local efficacy of the drug while

minimising systemic side effects (Raeburn and Woodman, 1994; Zhu et al., 2015a).

There are few published studies on engineering inhalable theophylline particles. A low-dose pressurised metered-dose inhaler (pMDI) formulation of theophylline (Zhu et al., 2015a) and formulations for dry powder inhalers (polymeric composite particles, microspheres, cocrystals and nanosized rods agglomerates) have been produced and characterised (Alhalaweh et al., 2013; Kadota et al., 2015; Momeni and Mohammadi, 2009; Salem et al., 2011; Zhang et al., 2009; Zhu et al., 2015b). Blends of theophylline microparticles (63-90 μm) with inhalable budesonide and terbutaline particles (< 5 μm) were proposed as a formulation approach for concurrent oral and pulmonary drug delivery with theophylline acting as a carrier (Salama et al., 2014).

DPIs have many advantages (inherent stability of dry powders, administration of high doses, short delivery times, the absence of propellants and breath-actuation) compared to other inhalation devices, namely pMDIs and nebulisers (Atkins, 2005).

The aim of the present work is to produce inhalable dry powder formulations of theophylline, by coupling wet bead milling in an organic solvent followed by spray drying of the milled suspension. The effect of mannitol addition during the wet milling of theophylline on the micromeritic, solid state and aerosol performance of the produced spray-dried particles was investigated. The experimental data of this study were complemented with a computational study of the interaction between theophylline and mannitol (i.e. crystal morphology modelling and lattice

matching calculations) in order to elucidate the role of mannitol as a co-milling agent.

2. MATERIALS AND METHODS

2.1 Materials

Theophylline (THEO), 3,7-dihydro-1,3-dimethyl-1H-purine-2,6-dione (LKT Laboratories, USA), was used as the drug under investigation. D-mannitol (MAN, Pearlitol 160C®, Roquette Freres, France) was used as co-milling agent and matrix former of the microcomposites. Isopropanol (IPA, Thermo Scientific, UK) was used as the milling medium for the preparation of suspensions. Methanol and water both from Fisher Scientific UK, and trifluoroacetic acid (TFA, Sigma-Aldrich Co., USA) were used for the HPLC analysis. All the solvents used were of analytical grade.

2.2 Methods

2.2.1 Preparation of suspensions

Suspensions were prepared by wet bead milling using a laboratory planetary mill (Pulverisette 5, Fritsch Co., Germany). 1.0 g of solids (THEO and MAN), 10 g of milling beads (0.5 mm diameter aluminum borosilicate glass grinding beads, Gerhardt Ltd, UK) were weighed into a glass vial of 14 ml capacity and suspended in 10 ml IPA, as the dispersing medium. The total concentration of solids (THEO and MAN) in suspension was kept constant (5% w/v) and different THEO to MAN mass ratios (i.e. 25:75, 50:50 and 75:25) were employed (Table 1). The vials were placed into a stainless steel milling pot with a maximum loading capacity of 8 pots. Rotation speed (300 rpm) and milling duration (6 cycles of altered

bowl rotation direction) were selected based on preliminary experiments. Each milling cycle comprised 60 min rotation followed by 20 min pause to cool down the milling vessels and to prevent overheating of the instrument's rotors. The suspensions were left to cool to room temperature and collected by withdrawal with a pipette to separate from the milling beads.

2.2.2 Preparation of spray-dried microcomposite particles

The obtained suspensions were diluted 1:2 with IPA, before spray-drying, to obtain suspensions with an overall solid concentration 5% w/v in IPA. Spray drying was performed with a Gea Niro Spray Dryer SD Micro™ (Gea Process Engineering, Denmark) operated with nitrogen as the drying gas. Inlet temperature of 80 ± 3 °C was selected, and atomizer gas flow and chamber inlet flow were set at 2.5 and 25 kg h^{-1}, respectively. The nozzle pressure was set at 1.5 bar and the bag filter pressure at 2.1 bar. The outlet temperature control was set at 20%, resulting in outlet temperature of 60 ± 5 °C.

2.2.3 Characterisation of spray-dried microcomposite particles

The spray-dried powders were characterised for: particle surface morphology and shape by scanning electron microscopy (SEM) and image analysis of the SEM images; particle size distribution (PSD) by laser diffractometry; specific surface area by Brunauer-Emmett-Teller (BET) method; solid state by X-ray powder diffraction (XRPD), Fourier transform infrared spectroscopy (FT-IR) and differential scanning calorimetry (DSC); drug loading by HPLC analysis of theophylline content and in vitro aerosol performance using the next generation impactor (NGI).

2.2.3.1 Scanning electron microscopy (SEM)

Samples were placed on a double-side electroconductive adhesive tape, which was fixed on an aluminum stub then coated with gold under argon atmosphere to a thickness of 10 nm (Quorum model 150). SEM micrographs were taken using a FEI Quanta 200 FEG ESEM (Netherlands), at 5.00 kV.

2.2.3.2 Image Analysis

SEM images were processed with the open source image processing software FIJI/Image J (Schindelin et al., 2012) to determine the number-based aspect ratio of the particles. The major and minor axis (i.e. primary and secondary axis of the best fitting ellipse) of a minimum of 100 particles was measured for each spray-dried powder and for the starting materials, and the aspect ratio was calculated as the ratio of the minor to the major axis.

2.2.3.3 Laser diffraction size analysis

HELOS/ BR laser diffractometer (Sympatec GmbH, Germany) fitted with the micro-dosing unit ASPIROS and combined with the dry disperser RODOS was employed. Samples were placed in the feeder and pressurised air of 4 bar was used to disperse them in the measurement chamber while the feeding velocity was constant at 50 mm sec^{-1}. An R2 lens detector (0.25- 87.5 µm) and the particle size distribution (PSD) analysis software Windox 5 were used.

The particle size distribution of the starting materials was measured with Malvern Mastersizer 3000 equipped with a dry sampling system (Aero S,

Malvern Instruments, UK), as the particle size range covered by this laser diffractometer is 0.1-3500 μm. The standard operating conditions used were: refractive index: 1.52, vibration feed rate: 25%, measurement time: 5 s, dispersive air pressure: 4 bar.

In all the cases, particle size parameters corresponding to the 10^{th}, 50^{th}, 90^{th} percentile of particles ($D_{10\%}$, $D_{50\%}$, $D_{90\%}$) were recorded.

2.2.3.4 Specific surface area and porosity

The specific surface area was measured using the nitrogen adsorption Brunauer-Emmett-Teller (BET) method with a Quantachrome Nova 4200e multi-station gas sorption surface area analyser (Quantachrome Ltd, UK) Approximately 0.1 g of each powder was placed in each sample cell, and the outgassing process was conducted at 105 ^{o} C over 2 h. The total pore volume and the average pore radius were calculated following the t-plot method.

2.2.3.5 X-ray powder diffractometry (XRPD)

XRPD patterns were obtained with a bench-top diffractometer (Rigaku Miniflex 600, Japan) to assess crystallinity. Cu Kα radiation at 15 mA and 40 kV with a step of 0.02 deg and a speed of 5 deg min^{-1} was used, covering a 2 theta of 3-40 ^{o}. Miniflex Guidance was the analysis software.

2.2.3.6 Fourier transform infrared spectroscopy (FT-IR)

Spectra of the starting materials, their physical mixtures and the microcomposites were recorded using a PerkinElmer Spectrum^{100} FT-IR

spectrometer equipped with the attenuated total reflection (ATR) sampling accessory. Samples were scanned at room temperature, at the transmission mode, over a wavenumber range of 4000-650 cm^{-1}, 16 accumulations and 1 cm^{-1} resolution. Before each measurement, a background spectrum of air was acquired under the same instrumental conditions. The acquired spectra were processed using the PerkinElmer Spectrum Express software (PerkinElmer, Inc., USA).

2.2.3.7 Differential scanning calorimetry (DSC)

DSC was performed using a TA DSC Q200 previously calibrated with indium. Weighed powder samples (1-3 mg) were sealed into crimped standard aluminum pans (TA) and heated under nitrogen flow (50 ml min^{-1}) from 25 °C to 30 °C above their melting point, at a heating rate of 10 °C min^{-1}.

2.2.3.8 Drug loading

5 mg of each spray-dried formulation were dissolved in 25 ml water and theophylline concentration was determined using an HPLC system (Agilent 1100 Series, Agilent Technologies, Germany) following the method described by Alhalaweh et al. (2013). The correlation coefficient of the calibration curve was R^2: 0.9997 for a concentration range of 5-400 μg ml^{-1}, indicating acceptable linearity.

2.2.3.9 In vitro aerosol performance

Deposition profiles were determined with Ph. Eur. Apparatus E (Next Generation Impactor, NGI, Copley Instruments Ltd, UK) fitted with a stainless steel 90^{O} induction port (IP) and a pre-separator (PS) operated

as specified in European Pharmacopoeia (Ph. Eur. 8th edition, monograph 2.9.18) and connected to a high-capacity vacuum pump (Model HCP5, Copley Instruments Ltd, UK). Prior to use, the impaction cups in each of the seven stages were coated with 1% w/v silicone oil solution in hexane, and allowed to dry for 1 h, in order to minimise 'particle bounce' and entrainment of particles between the stages. The final stage of the impactor, known as micro-orifice collector (MOC), was fitted with a fiberglass filter (nylon 0.45 μm, Millipore, UK). The flow rate was measured using a flow meter (Flow Meter Model DFM 2000, Copley Instruments Ltd, UK) prior to each run, to ensure that a flow of 60 L min^{-1} was achieved. Gelatin capsules (size 3) were filled with accurately weight amounts of product corresponding to about 10 mg of THEO. Following filling, capsules were stored in a desiccator over silica gel for 24h prior to performing the deposition study. Storage for 24h allowed relaxation of any electrical charge without influencing the brittleness of the capsules as their water content in preliminary studies was found to be inside the normal moisture specification limits (13-16% for gelatin). The inhaler device (Cyclohaler®) was connected to the impactor via an airtight rubber mouthpiece adaptor and tested at 60 L min^{-1} for an actuation time of 4 s. The capsules were discharged into the NGI, and after dispersion the powder deposited on the capsules, mouthpiece, inhaler and each NGI part was collected by exhaustively washing with water (HPLC grade) transferred into volumetric flasks and assayed. The HPLC conditions for the assay were identical to those for drug content determination. To characterise the aerosol performance the following parameters were determined: the emitted fraction (EF %) was calculated as the ratio of the

drug mass depositing in the mouthpiece, induction port, pre-separator, and impactor stages (1 to MOC) to the cumulative mass of drug collected following actuation (total drug deposited in the capsule, inhaler, mouthpiece, throat, pre-separator and stages). The fine particle fraction (FPF %) of each dose was the ratio of the drug mass depositing on stages 2 to MOC over the recovered dose. The fine particle dose (FPD) was calculated as the ratio of mass deposited on stage 2 to MOC, to the number of doses (n=3). Stage 2 had a cut-off diameter of 4.46 μm. The mass median aerodynamic diameter (MMAD) defined as the median particle diameter of the formulation deposited within the NGI, and the geometric standard deviation (GSD) determined as the square root of the ratio of the particle size at 84.13^{th} percentile to that of 15.87^{th} percentile. Both MMAD and GSD were determined from the linear region in the plot of the cumulative mass distribution versus the logarithm of aerodynamic diameters.

2.2.4. Statistical data analysis

An analysis of variance (one-way ANOVA) with Tukey's multiple comparison test was carried out to evaluate differences between the mean values using Prism 6 (GraphPad Software, Inc., USA). Probability values less than 0.05 were considered as indicative of statistically significant differences.

2.2.5. Computational study of the interaction between the crystals of theophylline and mannitol

In order to gain insight into the intermolecular interactions that influence the mechanical properties of theophylline and mannitol, the energetic and structural aspects of their crystals were investigated following a combination of approaches, namely: crystal morphology modelling, semi-classical density sums (SCDS-Pixel) and lattice matching calculations. Crystal structure coordinates for theophylline form II (CSD-REFCODE BAPLOT01, Ebisuzaki et al., 1997) and D-mannitol form β (CSD-REFCODE DMANTL07, Kaminsky and Glazer, 1997) were taken from the Cambridge Structural Database (Allen, 2002).

2.2.5.1 Crystal morphology modelling

The minimisation of the energy of the crystal lattice was performed using the General Utility Lattice Program (GULP v.4.3) (Gale and Rohl, 2003). The Dreiding 2.21 force field parameters (Mayo et al., 1990) were used in combination with high-quality electrostatic potential derived atomic point charges calculated at the 6-31G**/MP2 level of theory. For the determination of the atomic charges the Firefly quantum chemistry package was used (A. Granovsky, http://classic.chem.msu.su/gran/gamess/index.html), which is partially based on the GAMESS (US) source code (Schmidt et al., 1993). Crystal morphologies based on Bravais-Friedel-Donnay-Harker (BFDH) theory (which assumes that the slowest growing faces are those with the greatest interplanar spacing, d_{hkl}) were constructed in order to identify faces more likely to occur in the crystal. For the morphology calculations the GDIS program was utilized, serving as a graphical front end to the GULP software program (Fleming and Rohl, 2005).

2.2.5.2 Semi-classical density sums (SCDS-Pixel) calculations

The crystal structures were analysed using the PIXEL approach developed by Gavezzotti (Gavezzotti, 2005). This method provides quantitative determination of crystal lattice energies and pairwise intermolecular interactions, with a breakdown of these energies into coulombic, polarisation, dispersion and repulsion terms. For the derivation of PIXEL energies, the electron density of theophylline and mannitol were calculated at the 6-31G**/MP2 level of theory using the Firefly quantum chemistry package. Finally, energy vector diagrams were constructed according to Shishkin et al. (2012) using the processPIXEL package and the results were visualised using the Mercury software program (Bond, 2014; Macrae et al., 2008; Shishkin et al., 2012)

2.2.5.3 Computational Lattice Matching Calculations

Possible interactions between crystal faces of theophylline and mannitol were probed applying a computational lattice matching approach, using the Geometric Real-space Analysis of Crystal Epitaxy (GRACE) software (Mitchell et al., 2011). Cut-off distances of dc = 0.5 Å and d0 = 0.3 Å were selected. The value of θ was varied in the range of −90° to 90° with increments of 0.5°, and a search area of 400 × 400 Å and a range of overlayer *hkl* planes from $-3 \leq h, k, l \leq +3$ were employed. The epitaxy score, E, was calculated using the Gaussian function. The chemical complementarity at the geometrically matching crystal faces was evaluated by visual inspection of the crystal structures using the Mercury software program (Macrae et al., 2008).

3. RESULTS AND DISCUSSION

3.1 Preparation of microcomposite particles

Isopropanol (IPA) was selected as the wet milling medium based on preliminary solubility measurements. The lower solubility of anhydrous theophylline in IPA (2.81 ± 0.18 mg ml^{-1}, at 25 ° C for 24h) compared to its aqueous solubility (7.36 mg ml^{-1}, at 25 ° C, Yalkowsky and He, 2003) ensures the formation of nanocrystals that will be suspended in the liquid medium. Also, it may limit the risk of solution-mediated phase transformation that can give rise to increased amounts of amorphous form. Moreover, anhydrous theophylline is transformed to monohydrate when processed in water, while such hydration transition is not expected to occur in IPA.

Wet bead milling of anhydrous theophylline, in IPA, did not result in the production of nanosized particles, even after 6 h milling. By contrast, wet milling of mannitol in IPA resulted in submicron-sized particles as can be seen from the microcomposites obtained after spray drying of the suspension. The minor axis and major axis of the primary mannitol nanocrystals based on image analysis of SEM images and was found to be 405.44 ± 58.72 nm and 724.24 ± 113.46 nm, respectively. Therefore, use of isopropanol as the wet milling medium and mannitol as co-milling agent were selected.

The use of mannitol (MAN) as a co-grinding agent, enhancing the size reduction of drug particles and even leading to an increase in their bioavailability, has been reported previously (Kubo et al., 1996; Takahata

et al., 1992). However, in these earlier studies dry grinding techniques were used and the authors mainly focused on bioavailability studies in animals rather than on the mechanism underlying size reduction of drug particles in the presence of mannitol.

Mannitol is a commonly used matrix former during the solidification of aqueous nanosuspensions, for both oral and pulmonary drug delivery (Malamatari et al., 2016). It is usually incorporated prior to spray drying due to its high aqueous solubility, and forms a continuous matrix around the drug nanocrystals enhancing their redispresibility on rehydration (Chaubal and Popescu, 2008; Yue et al., 2013). It should be highlighted that in this study mannitol is not dissolved prior to spray drying but is added before the wet milling of anhydrous theophylline. So, both substances are in suspended form due to their marginal solubility in IPA. The total concentration of solids (THEO and MAN) in suspension was kept constant (5% w/v) and different THEO to MAN mass ratios (i.e. 25:75, 50:50 and 75:25) were employed (Table 1) in order to elucidate the potential effect on theophylline's particle size reduction, and also on the micromeritic, solid state and aerosolisation properties of the microcomposite particles produced.

3.2 Characterisation of microcomposite particles

3.2.1 Micromeritic properties

The SEM images of starting materials are presented in Fig.1. Anhydrous theophylline (THEO) particles consisted of primary crystallites bound together to form needle–shaped particles with a $D_{50\%}$ of 124.12 ± 18.33

μm. Mannitol particles also exhibited an elongated morphology, with a $D_{50\%}$ of 68.07 ± 1.36 μm (Table 2).

SEM images of the microcomposites produced by wet milling and spray drying are given in Fig.2. Wet milling of theophylline in the absence of mannitol followed by spray drying resulted in particles with smaller size compared to the raw drug, exhibiting a $D_{50\%}$ of 4.64 ± 0.87 μm and an aspect ratio of 0.41 ± 0.14, with values closer to 1 indicating a more spherical shape. The slight increase in the aspect ratio values of spray dried suspended theophylline (SD susp. THEO) compared to the raw material (0.33 ± 0.18) indicated the susceptibility of theophylline crystals to break along their short axis (Ho et al. 2012).

Simultaneous wet milling of theophylline and mannitol in isopropanol followed by spray drying resulted in microcomposite particles, which consist of theophylline and mannitol crystals assembled together (Fig.2). They exhibited $D_{50\%}$ values ranging from 3.5 to 2 μm, with size decreasing as mannitol content increased, and $D_{90\%}$ values below 10 μm making them suitable for pulmonary drug delivery (Table 2).

Moreover, inclusion of increasing amounts of mannitol produced particles with increased sphericity and porosity, demonstrated by the aspect ratio closer to 1 and higher specific surface area and pore volume values, respectively (Table 2 and 3). Thus, addition of mannitol during wet milling in isopropanol facilitated the size reduction of theophylline crystals and their assembly in microcomposites by forming porous and spherical agglomerates of mannitol nanocrystals in which submicron theophylline particles are embedded.

3.2.2 Solid state characterisation

The solid state of both theophylline and mannitol in the microcomposite formulations may change either during milling or spray drying. This was examined as different solid forms exhibit different physicochemical and mechanical properties, which may influence processability during product manufacturing and also drug stability, solubility, dissolution and ultimately therapeutic efficacy (Adeyeye et al., 1995; Raw et al., 2004).

Mannitol is known to be highly crystalline even during milling and spray drying. It exists in three polymorphic forms; alpha (α), beta (β) and delta (δ) (Fronczek et al., 2003). The β-form is the stable form of mannitol however both α- and δ-forms were found to be chemically and physically stable for at least 5 years when stored at 25 o C and 43% relative humidity (Burger et al., 2000). Preparation of mannitol particles by different methods (e.g. freeze drying, spray drying, jet milling or antisolvent crystallisation) as well as process parameters during spray drying (i.e. outlet temperature) have been reported to influence the solid form of D-mannitol (Kaialy and Nokhodchi, 2013; Maas et al., 2011; Tang et al., 2009).

XRPD is a fast and straightforward method for determining the basic information regarding the solid state of a powdered material with a limit of crystallinity detection in amorphous drug compositions around 5-10% (Stephenson et al., 2001). According to the XRPD patterns of the starting materials (Fig. 3), the diffraction peaks of anhydrous theophylline are characteristic of the form II (2 theta: 7.2 °, 12.6 °, 14.5 °) while for mannitol they are characteristic of the β form (2 theta: 14.7 °, 18.8 °,

23.6 °, 29.5 °). Similar results regarding the solid state of Pearlitol 160C®, the commercial type of mannitol used in our study, were reported in other studies (Cares-Pacheco et al., 2015; Hulse et al., 2009).

The XRPD pattern of the spray-dried microcomposites of THEO wet milled alone (SD susp. THEO) exhibited the same characteristic peaks as the starting material, indicating that both processes (i.e. wet milling coupled by spray drying) did not alter the polymorphic form of anhydrous theophylline (Fig. 3). Similarly, the spray-dried microcomposite of mannitol wet milled alone (SD susp. MAN) was in the same form as the raw material (form β) (Fig. 3).

For the microcomposites containing both THEO and MAN wet milled together in different mass ratios, the diffraction patterns shown in Fig. 3, were essentially a summation of the patterns of the starting materials. In all cases, reduction in the intensities and broadening of the peaks, compared to the patterns of the starting materials, can be attributed to the smaller size of the primary crystals in the microcomposite formulations and strain caused by the milling process (Hecq et al., 2005).

DSC was used to assess the thermal behaviour of the starting materials and the microcomposite formulations (Fig. 4). The DSC curve of the raw THEO showed an endothermic melting peak at 273 °C. The same thermal transition was observed for the SD susp. THEO formulation. The DSC of mannitol starting material (Pearlitol 160C®) and the SD susp. MAN showed one sharp endothermic peak at 167 °C that relates to the melting of mannitol crystals. Regarding the DSC curves of the microcomposite particles containing both THEO and MAN, instead of the expected two

endothermic events corresponding to the melting of the two components, a change in the thermal behaviour of theophylline was observed in the presence of mannitol. More specifically, after the melting of mannitol at around 165 ° C, theophylline appeared to dissolve completely in the melted mannitol when a drug load of up to 50%w/w was used, and partially at higher drug loads leading to the broadening of the melting peak of theophylline and a shift towards lower temperature (around 255 ° C) compared to the raw THEO material. However, as the FT-IR spectra of the physical mixtures and spray-dried suspensions of THEO and MAN presented the same bands as the raw materials (Fig. 5), it can be assumed that the interaction between theophylline and mannitol is limited to temperatures above the melting point of mannitol (166 ± 2°C). Similar results have been reported on the interaction of mannitol with other drugs (e.g. carbamazepine and promethazine hydrochloride) indicating that DSC should not be used alone to detect any inherent incompatibility between substances but it has to be combined with other non-thermal techniques, such as XRPD and FT-IR (Flicker et al., 2011; Joshi et al., 2002; Thumma and Repka, 2009).

Overall, the XRPD data suggest that the engineered microcomposite formulations retain their crystallinity during wet bead milling followed by spray drying. The preservation of the crystalline state is advantageous, ensuring the long-term physical stability of the formulations during storage. At this point, it should be highlighted, that dry milling techniques (e.g. air jet milling and ball milling) can induce crystal defects and even cause surface amorphisation of the particles (Ward and Schultz, 1995). These phenomena seem to be avoided during wet bead milling, as the

liquid medium ensures rapid recrystallisation of potentially formed amorphous regions (Kayaert and Van den Mooter, 2012). Another suggested mechanism is that the liquid media allows fast cooling during particle breakage, which can minimise formation of local hot spots on particle surfaces and thus reduce the extent of surface amorphisation (Monteiro et al., 2012).

3.2.3 Drug loading

The results of THEO content in microcomposites are given in Table 1. The assayed THEO content was close to the nominal, indicating no significant loss or powder segregation during the production processes. The small deviation of the assayed THEO amount compared to the theoretical value may be attributed to the suspension collection method employed at the end of the milling process. Separation by pipetting cannot achieve total suspension recovery with small amounts remaining among the beads. In industrial settings this is unlikely to be an issue as mills with separate holding and receiving tanks equipped with paddle mixers are used (Monteiro et al., 2012). In this way, enhanced suspension homogeneity and recovery are ensured leading to the production of formulations with consistent drug loading.

3.2.4 In vitro aerosol performance

The drug deposition profiles of the formulations produced are shown in Fig. 6, while parameters of their aerosol performance are given in Table 4.

The SD susp. THEO exhibited a significantly lower emitted fraction (EF%) of 65.6 ± 0.8 compared to the formulations containing mannitol ($p<0.05$), which may be attributed to the needle-shaped morphology. Elongated particles, despite their ability to travel further in the lung airway, were found to have poor dispersion from inhaler when administered as dry powders for inhalation as they are subject to strong attractive forces when in contact along their axis (Crowder et al., 2002). For the formulations containing mannitol reduced capsule and device retention was observed, leading to EF% around 80% for all the various theophylline to mannitol (THEO:MAN) ratios examined in this study (Table 4). This may be attributed to their more spherical size that allows them to leave the capsule and device by the additional mechanism of rolling.

Wet milling of theophylline in the presence of mannitol followed by spray drying resulted in particles with enhanced aerosol performance as demonstrated by the higher fine particle fraction (FPF%) and fine particle doses (FPD) achieved compared to the SD susp. THEO. More specifically, the SD susp. THEO achieved a FPF of 26.1 ± 7.1 % and a mass median aerodynamic diameter (MMAD) of 4.5 ± 1.1 μm while incorporation of mannitol resulted in approximately 2- fold increase in FPF% ($p<0.01$), depending on the drug to mannitol ratio, and in MMADs close to 3 μm for the respective formulations (Table 4). Increasing the concentration of mannitol from 25% to 50% w/w or 75% w/w resulted in slightly higher FPF% however the increase was not found statistically significant ($p>0.05$). Moreover, increasing mannitol concentration shifted drug

deposition from stages 2 and 3 to lower stages of the impactor (i.e. stages 4 to 6) (Fig. 6).

It is known, that the aerodynamic diameter, which is a function of the geometric size and particle density, governs the behaviour of a particle in the airstream. Thus, the improved aerosolisation efficiency of the formulations containing mannitol may be attributed to their smaller particle size and increased porosity compared to SD susp. THEO (Table 2 and 3).

Previously, when mannitol was added as a matrix former in aqueous nanosuspensions prior to the spray-drying step it was found to have no significant influence on the surface roughness and aerosol performance of the nano-matrix powders produced (Yamasaki et al., 2011). This result, which at first sight seems contradictory to our conclusions, can be explained by the fact that mannitol was dissolved in the aqueous drug nanosuspensions and during spray drying it formed a continuous matrix around the drug nanocrystals. In our case, mannitol nanocrystals were suspended in isopropanol prior to the spray-drying step, and after solvent evaporation they formed porous agglomerates wherein theophylline particles were embedded.

3.3 Computational study of the interactions between theophylline and mannitol

Results of PIXEL calculations for theophylline form II and mannitol form β are given in Table 5. Results on the mechanical properties of the crystals,

calculated by molecular mechanics force field methods are presented in Table 6. Regarding the energy decomposition results for theophylline (Table 5), only the repulsive component is destabilising with all the other energy terms to contribute to the crystal lattice stabilisation. More specifically, the dispersion and coulombic components have almost equal contributions regarding the stabilisation. These results are in agreement with previously published data (Dunitz and Gavezzotti, 2005). In the case of mannitol, the coulombic component is by far the most important stabilising interaction, reflecting the significance of the hydrogen bonds in the stabilisation of the crystal structure.

The crystal morphologies of theophylline and mannitol, determined according to the BFDH theory and energy vector diagrams are shown in Fig. 7. From Fig. 7c, it is seen that, as already described by Dunitz and Gavezzotti (2005), theophylline forms stacked dimers, but those dimmers do not form layers in the crystal structure, and there are strings of N-H···N hydrogen bonds between non-coplanar molecules. The direction of (stabilising) coulombic and polarisation, as well as the (destabilising) exchange repulsion interaction forces, coincides with the hydrogen bonding motif. On the other hand, the (stabilising) dispersion interaction forces extend mainly between adjacent coplanar purine rings, normal to the plane defined by the N-H···N hydrogen bond strings.

The spatial arrangement of the interaction forces in the lattice of theophylline defines the (200) plane as the most probable slip direction since no significant interaction forces act along or intersect this plane. However, as it becomes evident from the calculated crystal morphology in

order to cause shearing of the crystal along the (200) plane, a force has to act on the much smaller (110) or (201) faces (Fig.7a). The small relative surface area of these crystal faces, which is expected to get gradually smaller as milling proceeds, together with the rather high stiffness of its crystal structure (relatively high values of Young's modulus, Table 6) is probably the cause of the difficulty to break theophylline crystals by milling.

Mannitol exhibits a needle-like habit, with elongation along the a crystallographic axis, which is adequately represented by the BFDH morphology model, Fig. 7b. As demonstrated by the energy vector diagram of mannitol (Fig. 7d), intermolecular interaction forces extend parallel to the c crystallographic axis, clearly defining a slip direction along the (020) plane, in agreement with literature data (Al-Khattawi et al., 2015; Ho et al., 2012). Moreover it has been reported that mannitol crystals also fracture along the (011) plane (Ho et al. 2012). According to the energy vector diagram of mannitol, strong stabilising forces act along this plane, therefore fracture should not be very likely. However, when the elongated habit of the crystals is taken into account, it becomes evident that mechanical forces normal to the elongation axis eventually prevail and cause fracture.

Regarding the mechanism by which mannitol facilitates the size reduction of theophylline, this may be attributed to the interaction between certain crystal faces of the two substances, leading to subsequent adsorption-induced reduction of strength of a solid (AIRS); a phenomenon of physicochemical mechanics also known as Rehbinder effect (Rehbinder

and Shchukin, 1972). According to Rehbinder, adsorption of additives on the surface of the particles can make crack propagation easier by way of reduction in surface energy (Andrade et al., 1950).

In order to investigate potential interactions between crystal faces of theophylline and mannitol, geometric lattice matching calculations were employed. It should be noted that geometric lattice matching calculations are developed to study epitaxial growth (i.e. growth of one crystal (overlayer) on the surface of another crystal (the substrate), on which the growth of the overlayer is oriented by the lattice structure of the substrate) (Datta and Grant, 2004). However, as the epitaxy score relates to the density and precision of lattice coincidence within a predefined search area and the higher its value, the larger the area a substrate and an overlayer can maintain a favourable low energy interaction, we extended the use of these calculations in our case (Lee et al., 2010).

No significant geometric matching was found between the (200) plane of theophylline and (020) plane of mannitol. On the contrary, a high E value, the epitaxy score, indicates good matching between the (200) plane of theophylline and the (011) plane of mannitol. The value of the best matching theta, the angle between the (200) plane of theophylline and the (011) plane of mannitol is -79.5 ^{o} with an E value of 5.4895 (Fig. 8a). A one-dimension Moiré plot shows a high degree of superimposed patterns for theophylline's (200) and mannitol's (011) crystal plane, which is typical of registry between the two crystal lattices (Fig. 8b).

The geometric matching of the lattice planes provides an indication of favourable interactions that could also lead to attachment of one crystal

on the other, initiating processes involved in the adsorption-induced reduction of strength of theophylline particles. These results, together with the different physicomechanical properties of the compounds may shed light on the mechanisms behind the enhancement of theophylline's particle size reduction by mannitol during wet milling.

4. CONCLUSIONS

Inhalable-sized particles of theophylline with various amounts of mannitol were successfully prepared by wet milling in isopropanol followed by spray drying. The addition of mannitol as a co-milling agent facilitated the size reduction of theophylline needle-like crystals and resulted in microcomposite particles which consisted of theophylline and mannitol submicron crystals assembled together. The microcomposites were found to be in the same crystalline state as the starting material(s). Increasing the proportion of mannitol was found to result in the production of smaller, more spherical and porous particles with enhanced aerosol performance. Crystal morphology modelling and geometric lattice calculations were useful tools providing an insight into the intermolecular interactions that may influence the mechanical properties of theophylline and mannitol and the role of the latter as a co-milling agent. Overall, wet milling of drugs in an organic solvent in the presence of mannitol, followed by spray drying, can be used a formulation approach for the production of respirable particles of water-soluble drugs or drugs that are prone to crystal transformation in an aqueous environment (i.e. formation of hydrates). Preservation of the solid phase makes this approach preferable to micronisation by dry milling techniques, which is associated with

limitations, such as drug amorphisation and performance variability.

5. ACKNOWLEDGEMENTS

EPSRC Centre of Doctoral Training in Targeted Therapeutics and Formulation Sciences for the funding (EP/I01375X/1). Mr David McCarthy (UCL) for taking the SEM images. Dr Dimitrios Fatouros and Mr Georgios Eleftheriadis (Aristotle University of Thessaloniki) for carrying out the BET measurements.

Graham Buckton, Kevin Taylor and Satyanarayana Somavarapu would like to pay tribute to the enormous contribution Sandy Florence has made to the pharmaceutical sciences and pharmacy education, and thank him for his generous support, encouragement and leadership throughout their careers.

6. REFERENCES

Adeyeye, C.M., Rowley, J., Madu, D., Javadi, M., Sabnis, S.S., 1995. Evaluation of crystallinity and drug release stability of directly compressed theophylline hydrophilic matrix tablets stored under varied moisture conditions. Int. J. Pharm. 116, 65–75.

Al-Khattawi, A., Koner, J., Rue, P., Kirby, D., Perrie, Y., Rajabi-Siahboomi, A., Mohammed, A.R., 2015. A pragmatic approach for engineering porous mannitol and mechanistic evaluation of particle performance. Eur. J. Pharm. Biopharm. 94, 1–10.

Alhalaweh, A., Kaialy, W., Buckton, G., Gill, H., Nokhodchi, A., Velaga, S.., 2013. Theophylline Cocrystals Prepared by Spray Drying: Physicochemical Properties and Aerolisolization Performance. AAPS PharmSci Tech. 14, 265–276.

Allen, F.H., 2002. The Cambridge Structural Database: A quarter of a million crystal structures and rising. Acta Crystallogr. Sect. B Struct. Sci. 58, 380–388.

Andrade, E.N.D.C., Randall, R.F.Y., Makin, M.J., 1950. The Rehbinder Effect. Proc. Phys. Soc. Sect. B 63, 990–995.

Atkins, P.J., 2005. Dry powder inhalers: An overview. Respir. Care. 50, 1304-1312.

Barnes, P.J., 2013. Theophylline. Am. J. Respir. Crit. Care Med. 188, 901–906.

Barnes, P.J., 2008. Frontrunners in novel pharmacotherapy of COPD. Curr. Opin. Pharmacol. 8, 300–7.

Barnes, P.J., 2003. Therapy of chronic obstructive pulmonary disease. Pharmacol. Ther. 97, 87–94.

Bond, A.D., 2014. processPIXEL: a program to generate energy-vector models from Gavezzotti's PIXEL calculations. J. Appl. Crystallogr. 47, 1777–1780.

Bosch, H.W., Ostrander, K.D., Cooper, E.R., 1999. Aerosols Comprising Nanoparticle Drugs, patent no: WO/27363.

Brodka-Pfeiffer, K., Langguth, P., Graβ, P., Häusler, H., 2003. Influence of mechanical activation on the physical stability of salbutamol sulphate. Eur. J. Pharm. Biopharm. 56, 393–400.

Cares-Pacheco, M.G., Calvet, R., Vaca-Medina, G., Rouilly, a., Espitalier, F., 2015. Inverse gas chromatography a tool to follow physicochemical modifications of pharmaceutical solids: Crystal habit and particles size surface effects. Int. J. Pharm. 494, 113–126.

Chaubal, M. V, Popescu, C., 2008. Conversion of nanosuspensions into dry powders by spray drying: a case study. Pharm. Res. 25, 2302–2308.

Chow, A.H.L., Tong, H.H.Y., Chattopadhyay, P., Shekunov, B.Y., 2007. Particle engineering for pulmonary drug delivery. Pharm. Res. 24, 411–437.

Crowder, T.M., Rosati, J. a, Schroeter, J.D., Hickey, A.J., 2002. Fundamental effects of particle morphology on lung delivery : Predictions of Stoke's law and the particular relevance to dry powder inhaler formulation and development. Pharm. Res. 19,239-245.

Datta, S., Grant, D.J.W., 2004. Crystal structures of drugs: advances in determination, prediction and engineering. Nat Rev Drug Discov 3, 42–57.

Dunitz, J.D., Gavezzotti, A., 2005. Molecular recognition in organic crystals: Directed intermolecular bonds or nonlocalized bonding? Angew. Chemie - Int. Ed. 44, 1766–1787.

Duret, C., Wauthoz, N., Sebti, T., Vanderbist, F., Amighi, K., 2012. New inhalation-optimized itraconazole nanoparticle-based dry powders for the treatment of invasive pulmonary aspergillosis. Int. J. Nanomedicine 7, 5475–5489.

Ebisuzaki, Y., Boyle, P.D., Smith, J.A., 1997. Methylxanthines .1. Anhydrous theophylline. Acta Crystallogr. Sect. C - Cryst. Struct. Commun. 53, 777–779.

Fleming, S., Rohl, A., 2005. GDIS: A visualization program for molecular and periodic systems. Zeitschrift fur Krist. 220, 580–584.

Flicker, F., Eberle, V.A., Betz, G., 2011. Variability in commercial carbamazepine samples - Impact on drug release. Int. J. Pharm. 410, 99–106.

Fronczek, F.R., Kamel, H.N., Slattery, M., 2003. Three polymorphs (alpha, beta, and delta) of D-mannitol at 100 K. Acta Crystallogr. C. 59, 567–570.

Fucke, K., McIntyre, G.J., Wilkinson, C., Henry, M., Howard, J.A.K., Steed, J.W., 2012. New Insights into an Old Molecule: Interaction Energies of Theophylline Crystal Forms. Cryst. Growth Des. 12, 1395–1401.

Gale, J.D., Rohl, A.L., 2003. The General Utility Lattice Program (GULP). Mol. Simul. 29, 291–341.

Gavezzotti, a, 2005. Calculations of lattice energies of organic crystals: the PIXEL integration method in comparison with more traditional methods. Zeitschrift fur Krist. 220, 499–510.

Hecq, J., Deleers, M., Fanara, D., Vranckx, H., Amighi, K., 2005. Preparation and characterization of nanocrystals for solubility and dissolution rate enhancement of nifedipine. Int. J. Pharm. 299, 167–177.

Hirano, T., Yamagata, T., Gohda, M., Yamagata, Y., Ichikawa, T., Yanagisawa, S., Ueshima, K., Akamatsu, K., Nakanishi, M., Matsunaga, K., Minakata, Y., Ichinose, M., 2006. Inhibition of reactive nitrogen species production in COPD airways: comparison of inhaled corticosteroid and oral theophylline. Thorax 61, 761–766.

Ho, R., Naderi, M., Heng, J.Y.Y., Williams, D.R., Thielmann, F., Bouza, P., Keith, A.R., Thiele, G., Burnett, D.J., 2012. Effect of milling on particle shape and surface energy heterogeneity of needle-Shaped crystals. Pharm. Res. 29, 2806–2816.

Hong, J.., Oort, M.M.., 2011. Aggregate nanoparticulate medicament formulations, manufacture and use thereof. EP2627317 A2.

Hulse, W.L., Forbes, R.T., Bonner, M.C., Getrost, M., 2009. The characterization and comparison of spray-dried mannitol samples. Drug Dev. Ind. Pharm. 35, 712–718.

Joshi, B. V, Patil, V.B., Pokharkar, V.B., 2002. Compatibility studies between carbamazepine and tablet excipients using thermal and non-thermal methods. Drug Dev. Ind. Pharm. 28, 687–694.

Kadota, K., Nishimura, T., Hotta, D., Tozuka, Y., 2015. Preparation of composite particles of hydrophilic or hydrophobic drugs with highly branched cyclic dextrin via spray drying for dry powder inhalers. Powder Technol. 283, 16–23.

Kaialy, W., Nokhodchi, A., 2013. Freeze-dried mannitol for superior pulmonary drug delivery via dry powder inhaler. Pharm Res 30, 458–477.

Kayaert, P., Van den Mooter, G., 2012. Is the amorphous fraction of a dried nanosuspension caused by milling or by drying? A case study with Naproxen and Cinnarizine. Eur. J. Pharm. Biopharm. 81, 650–656.

Kim, A.I., Akers, M.J., Nail, S.L., 1998. The physical state of mannitol after freeze-drying: Effects of mannitol concentration, freezing rate, and a noncrystallizing cosolute. J. Pharm. Sci. 87, 931–935.

Kubo, H., Osawa, T., Takashima, K., Mizobe, M., 1996. Enhancement of oral bioavailability and pharmacological effect of 1-(3,4-dimethoxyphenyl)-2,3-bis(methoxycarbonyl)-4-hydroxy-6,7,8-trimethoxynaphthalene (TA-7552), a new hypocholesterolemic agent, by micronization in co-ground mixture with D-mannitol. Biol Pharm Bull 19, 741–7.

Labiris, N.R., Dolovich, M.B., 2003. Pulmonary drug delivery. Part II: the role of inhalant delivery devices and drug formulations in therapeutic effectiveness of aerosolized medications. Br. J. Clin. Pharmacol. 56, 600–12.

Lee, E.H., Boerrigter, S.X.M., Byrn, S.R., 2010. Epitaxy of a structurally related compound on the (100) faces of flufenamic acid form i and iii single crystals. Cryst. Growth Des. 10, 518–527.

Maas, S.G., Schaldach, G., Littringer, E.M., Mescher, A., Griesser, U.J., Braun, D.E., Walzel, P.E., Urbanetz, N. a., 2011. The impact of spray drying outlet temperature on the particle morphology of mannitol. Powder Technol. 213, 27–35.

Macrae, C.F., Bruno, I.J., Chisholm, J. a., Edgington, P.R., McCabe, P., Pidcock, E., Rodriguez-Monge, L., Taylor, R., Van De Streek, J., Wood, P.A., 2008. Mercury CSD 2.0 - New features for the visualization and investigation of crystal structures. J. Appl. Crystallogr. 41, 466–470.

Malamatari, M., Somavarapu, S., Bloxham, M., Buckton, G., 2015. Nanoparticle agglomerates of indomethacin: The role of poloxamers and matrix former on their dissolution and aerosolisation efficiency. Int. J. Pharm. 495, 516–526.

Malamatari, M., Somavarapu, S., Taylor, K.M.G., Buckton, G., 2016. Solidification of nanosuspensions for the production of solid oral dosage forms and inhalable dry powders. Expert Opin. Drug Deliv.

null–null. doi:10.1517/17425247.2016.1142524

Mayo, S.L., Olafson, B.D., Goddard, W.A., 1990. DREIDING: a generic force field for molecular simulations. J. Phys. Chem. 94, 8897–8909.

Mitchell, J., Bauer, R., Lyapustina, S., Tougas, T., Glaab, V., 2011. Non-impactor-based methods for sizing of aerosols emitted from orally inhaled and nasal drug products (OINDPs). AAPS PharmSciTech 12, 965–88.

Momeni, A., Mohammadi, M.H., 2009. Respiratory delivery of theophylline by size-targeted starch microspheres for treatment of asthma. J. Microencapsul. 26, 701–10.

Monteiro, A., Afolabi, A., Bilgili, E., 2012. Continuous production of drug nanoparticle suspensions via wet stirred media milling: a fresh look at the Rehbinder effect. Drug Dev. Ind. Pharm. 39, 1–18.

Pilcer, G., Vanderbist, F., Amighi, K., 2009. Spray-dried carrier-free dry powder tobramycin formulations with improved dispersion properties. J. Pharm. Sci. 98, 1463–75.

Pomázi, A., Buttini, F., Ambrus, R., Colombo, P., Szabó-Révész, P., 2013. Effect of polymers for aerolization properties of mannitol-based microcomposites containing meloxicam. Eur. Polym. J. 49, 2518–2527.

Raeburn, D., Woodman, V.R., 1994. Effect of Theophylline Administered Intratracheally as a Dry Powder Formulation on Bronchospasm and Airway Microvascular Leakage in the Anaesthetized Guinea-pig. Pulm. Pharmacol. 7, 243–249.

Raw, A.S., Furness, M.S., Gill, D.S., Adams, R.C., Holcombe Jr., F.O., Yu, L.X., 2004. Regulatory considerations of pharmaceutical solid polymorphism in Abbreviated New Drug Applications (ANDAs). Adv Drug Deliv Rev 56, 397–414.

Rehbinder, P.A., Shchukin, E.D., 1972. Surface phenomena in solids during deformation and fracture processes, in Davison, S.G. (Ed.), Progress in Surface Science, Pergamon, Oxford, pp. 97-188.

Salama, R.O., Young, P.M., Traini, D., 2014. Concurrent oral and inhalation drug delivery using a dual formulation system: the use of oral theophylline carrier with combined inhalable budesonide and terbutaline. Drug Deliv. Transl. Res. 4, 256–67.

Salem, H., Abdelrahim, M., Eid, K.A., Sharaf, M., 2011. Nanosized rods agglomerates as a new approach for formulation of a dry powder inhaler. Int. J. Nanomedicine 6, 311–320.

Schindelin, J., Arganda-Carreras, I., Frise, E., Kaynig, V., Longair, M.,

Pietzsch, T., Preibisch, S., Rueden, C., Saalfeld, S., Schmid, B., Tinevez, J.-Y., White, D.J., Hartenstein, V., Eliceiri, K., Tomancak, P., Cardona, A., 2012. Fiji: an open-source platform for biological-image analysis. Nat. Methods 9, 676–682.

Schmidt, M.W., Baldridge, K.K., Boatz, J. a, Elbert, S.T., Gordon, M.S., Jensen, J.H., Koseki, S., Matsunaga, N., Nguyen, K. a, Shyjun, S.U., Dupuis, M., Montgomery, J. a, 1993. General Atomic and Molecular Electronic Structure System. Building 14, 1347–1363.

Seton, L., Khamar, D., Bradshaw, I.J., Hutcheon, G. a., 2010. Solid state forms of theophylline: Presenting a new anhydrous polymorph. Cryst. Growth Des. 10, 3879–3886.

Shishkin, O., Medvediev, V., Zubatyuk, R., 2012. Supramolecular architecture of molecular crystals possessing shearing mechanical properties: columns versus layers. CrystEngComm 160–167.

Stephenson, G. a., Forbes, R. a., Reutzel-Edens, S.M., 2001. Characterization of the solid state: Quantitative issues. Adv. Drug Deliv. Rev. 48, 67–90.

Takahata, H., Nishioka, Y., Osawa, T., 1992. Micronization of poorly water soluble drug to submicron size by mixing grinding with low-molecular water-soluble crystalline. Funtai to Kogyo 24, 53–59.

Tang, P., Chan, H.K., Chiou, H., Ogawa, K., Jones, M.D., Adi, H., Buckton, G., Prud'homme, R.K., Raper, J. a., 2009. Characterisation and aerosolisation of mannitol particles produced via confined liquid impinging jets. Int. J. Pharm. 367, 51–57.

Thumma, S., Repka, M.A., 2009. NoCompatibility studies of promethazine hydrochloride with tablet excipients by means of thermal and non-thermal methods. Pharmazie 64, 183–189.

Tilley, S.L., 2011. Methylxanthines in asthma. Handb. Exp. Pharmacol. 439–456.

Ward, G.H., Schultz, R.K., 1995. Process-induced crystallinity changes in albuterol sulfate and its effect on powder physical stability. Pharm. Res.

Willart, J.F., Caron, V., Descamps, M., 2007. Transformations of crystalline sugars upon milling. J. Therm. Anal. Calorim. 90, 125–130.

Yalkowsky, S.H., He, Y., 2003. Handbook of Aqueous Solubility. CRC Press.

Yamasaki, K., Kwok, P.C.L., Fukushige, K., Prud'homme, R.K., Chan, H.-K., 2011. Enhanced dissolution of inhalable cyclosporine nano-matrix particles with mannitol as matrix former. Int. J. Pharm. 420, 34–42.

Yue, P.-F., Li, Y., Wan, J., Yang, M., Zhu, W.-F., Wang, C.-H., 2013. Study

on formability of solid nanosuspensions during nanodispersion and solidification: I. Novel role of stabilizer/drug property. Int. J. Pharm. 454, 269–277.

Zhang, W., Zhou, H., Chen, X., Tang, S., Zhang, J., 2009. Biocompatibility study of theophylline/chitosan/β-cyclodextrin microspheres as pulmonary delivery carriers. J. Mater. Sci. Mater. Med. 20, 1321–1330.

Zhu, B., Haghi, M., Goud, M., Young, P.M., Traini, D., 2015a. The formulation of a pressurized metered dose inhaler containing theophylline for inhalation. Eur. J. Pharm. Sci. 76, 68–72.

Zhu, B., Haghi, M., Nguyen, A., Goud, M., Yeung, S., Young, P.M., Traini, D., 2015b. Delivery of theophylline as dry powder for inhalation. Asian J. Pharm. Sci. 10, 520–527.

TABLES

Table 1. Nominal composition and assayed theophylline content (% w/w) of microcomposite particles together with the calculated drug loading efficiency (%) (mean ± SD, n=3).

Table 2. Particle size distribution data, aspect ratio values of the starting materials and microcomposite formulations containing different theophylline to mannitol ratios (mean ± SD, n=3).

Table 3. Specific surface area, total pore volume and average pore radius of the starting materials and microcomposite formulations containing different theophylline to mannitol ratios (n=3)*.

Table 4. Aerodynamic parameters of microcomposite formulations containing different theophylline to mannitol ratios using the Cyclohaler® at 60L min^{-1} (mean ± SD, n=3).

Table 5. Lattice energy (kJ/mol) decomposition according to the PIXEL scheme, for theophylline form II and mannitol form β. E_{COUL}: coulombic; E_{POL}: polarisation; E_{DISP}: dispersion; E_{REP}: repulsion and E_{TOTAL}: total intermolecular interaction energy.

Table 6. Calculated mechanical properties of theophylline form II and D-mannitol form β.

Table 3. Nominal composition and assayed theophylline content (% w/w) of microcomposite particles together with the calculated drug loading efficiency (%) (mean ± SD, n=3).

Formulation	Content (% w/w)			Drug loading efficiency (%)
	Nominal		Assayed	
	THEO	Mannitol	THEO	
SD susp. THEO	100	-	n/a	n/a
SD susp. THEO:MAN 75:25	75	25	76.2 ± 0.1	101.6 ± 0.1
SD susp. THEO:MAN 50:50	50	50	53.3 ± 0.1	106.7 ± 0.1
SD susp. THEO:MAN 25:75	25	75	28.7 ± 0.2	114.1 ± 1.0
SD susp. MAN	-	100	n/a	n/a

Table 2. Particle size distribution data and aspect ratio values of the starting materials and microcomposite formulations containing different theophylline to mannitol ratios (mean ± SD, n=3).

Formulation	Size distribution: d_{10}, d_{50}, d_{90} (4 bar, 50 mm s^{-1})			Image analysis
	$D_{10\%}$(µm)	$D_{50\%}$ (µm)	$D_{90\%}$ (µm)	Aspect ratio
THEO	29.90 ± 1.76	124.12 ± 18.33	352.27 ± 54.75	0.33 ± 0.18
Mannitol	12.23 ± 0.34	68.07 ± 1.36	208.13 ± 3.96	0.58 ± 0.21
SD susp. THEO	1.17 ± 0.31	4.64 ± 0.87	13.80 ± 4.60	0.41 ± 0.14
SD susp. THEO:MAN 75:25	0.97 ± 0.06	3.52 ± 0.68	9.72 ± 2.40	0.55 ± 0.15
SD susp. THEO:MAN 50:50	0.82 ± 0.05	2.95 ± 0.64	7.91 ± 1.95	0.68 ± 0.19
SD susp. THEO:MAN 25:75	0.61 ± 0.08	2.18 ± 0.30	5.11 ± 1.22	0.71 ± 0.12
SD susp. MAN	0.58 ± 0.03	2.86 ± 0.12	6.39 ± 0.50	0.85 ± 0.09

Table 3. Specific surface area, total pore volume and average pore radius of the starting materials and microcomposite formulations containing different theophylline to mannitol ratios (n=3)*.

Formulation	BET Surface area ($m^2\ g^{-1}$)	Total Pore Volume ($cc\ g^{-1}$) $x10^3$	Average Pore Radius (Å)
THEO	0.80	2.31	24.11
Mannitol	0.36	1.26	11.39
SD susp. THEO	5.23	8.63	21.82
SD susp. THEO:MAN 75:25	8.97	14.71	32.79
SD susp. THEO:MAN 50:50	9.64	20.14	41.77
SD susp. THEO:MAN 25:75	11.57	25.99	44.93
SD susp. MAN	19.73	39.13	39.67

* Relative standard deviation <4%

Table 4. Aerodynamic parameters of microcomposite formulations containing different theophylline to mannitol ratios delivered using the Cyclohaler® at 60L min^{-1} (mean ± SD, n=3).

Formulation	Emitted fraction (EF %)	Fine particle fraction (FPF %)	Fine particle dose (FPD, mg)	Mass median aerodynamic diameter (MMAD, μm)	Geometric Standard Deviation (GSD)
SD susp. THEO	65.6 ± 0.8	26.1 ± 7.1	2.6 ± 0.6	4.5 ± 1.1	1.7 ± 0.1
SD susp. THEO:MAN 75:25	84.0± 0.4	47.9 ± 2.3	4.8 ± 0.2	3.1 ± 0.2	1.6 ± 0.1
SD susp. THEO:MAN 50:50	78.9 ± 12.9	56.1 ± 0.8	5.6 ± 0.1	3.2 ± 0.3	1.6 ± 0.0
SD susp. THEO:MAN 25:75	84.1 ± 4.6	56.8 ± 8.7	5.7 ± 0.9	2.9 ± 0.1	1.7 ± 0.1

Table 5. Lattice energy (kJ/mol) decomposition according to the PIXEL scheme, for theophylline form II and mannitol form β. E_{COUL}: coulombic; E_{POL}: polarisation; E_{DISP}: dispersion; E_{REP}: repulsion and E_{TOTAL}: total intermolecular interaction energy.

Substance	E_{COUL}	E_{POL}	E_{DISP}	E_{REP}	E_{TOTAL}	ΔH_{SUB}
THEO	-95.5	-47.5	-109.0	123.2	-128.9	135.0*
Mannitol	-312.7	-139.7	-132.2	356.7	-227.8	202.0*

*Sublimation enthalpies (ΔH_{SUB}) were taken from http://webbook.nist.gov/chemistry

Table 6. Calculated mechanical properties of theophylline form II and D-mannitol form β.

	THEO	Mannitol
Bulk modulus (GPa)	14.81	10.85
Shear modulus (GPa)	4.59	4.15
Compressibility (GPa^{-1})	0.0675	0.0922
Young modulus (GPa)		
Ex	18.6	75.6
Ey	15.5	15.1
Ez	22.0	20.5

FIGURES

Figure 1. SEM images of starting materials.

Figure 2. SEM of microcomposite formulations containing theophylline and mannitol wet milled alone and in different mass ratios.

Figure 3. XRPD patterns of starting materials and microcomposite formulations containing different theophylline to mannitol ratios.

Figure 4. DSC thermograms of starting materials and microcomposite formulations containing different theophylline to mannitol ratios.

Figure 5. FT-IR spectra of starting materials, physical mixture (PM) of theophylline and mannitol (mass ratio 50:50) and SD susp. THEO:MAN 50:50.

Figure 6. Drug deposition profiles of microcomposites containing different theophylline to mannitol ratios using the Cyclohaler® at 60L min^{-1} (mean + SD, n=3). St.1-St.7 denote stages 1-7 of the NGI, the aerodynamic cut-off diameter of each stage is given in parenthesis.

Figure 7. Chemical structures and crystal morphologies of (a) theophylline anhydrous form II and (b) D-mannitol β form. Crystal morphologies are calculated according to the BFDH theory showing the orientation of the unit cell in the bulk crystal. Energy vector diagrams of (c) theophylline form II showing the direction of coulombic and polarisation (pink) and dispersion (yellow) interactions, and of (d) D-mannitol β form, showing the direction of combined stabilising (pink) and destabilising repulsive (green) interactions. Red surfaces indicate the most probable slip planes.

Figure 8. (a) Epitaxy score *vs* rotation angle and (b) Moiré patterns for the geometric matching of theophylline's (100) on mannitol's (011) crystal plane.

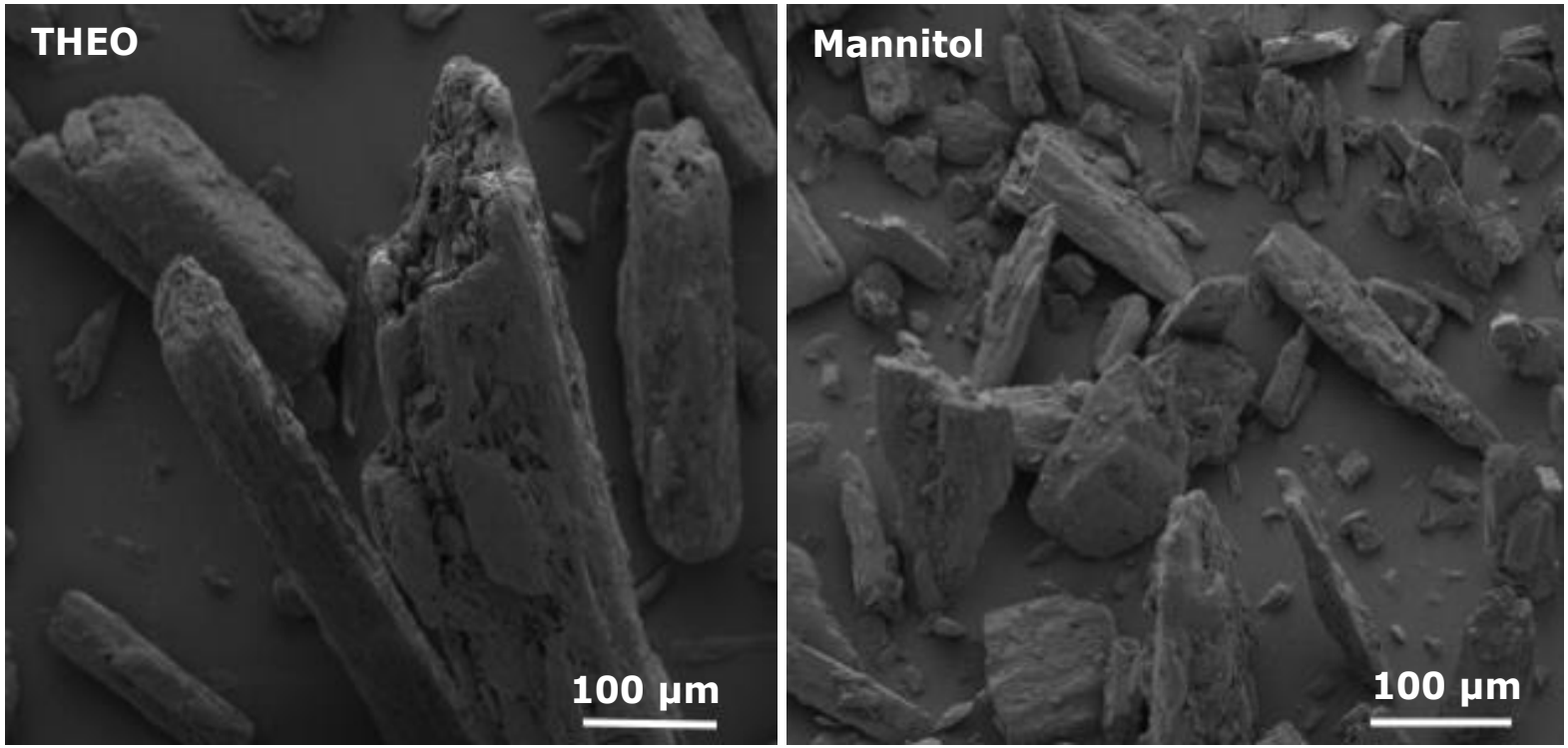

Figure 1. SEM images of starting materials.

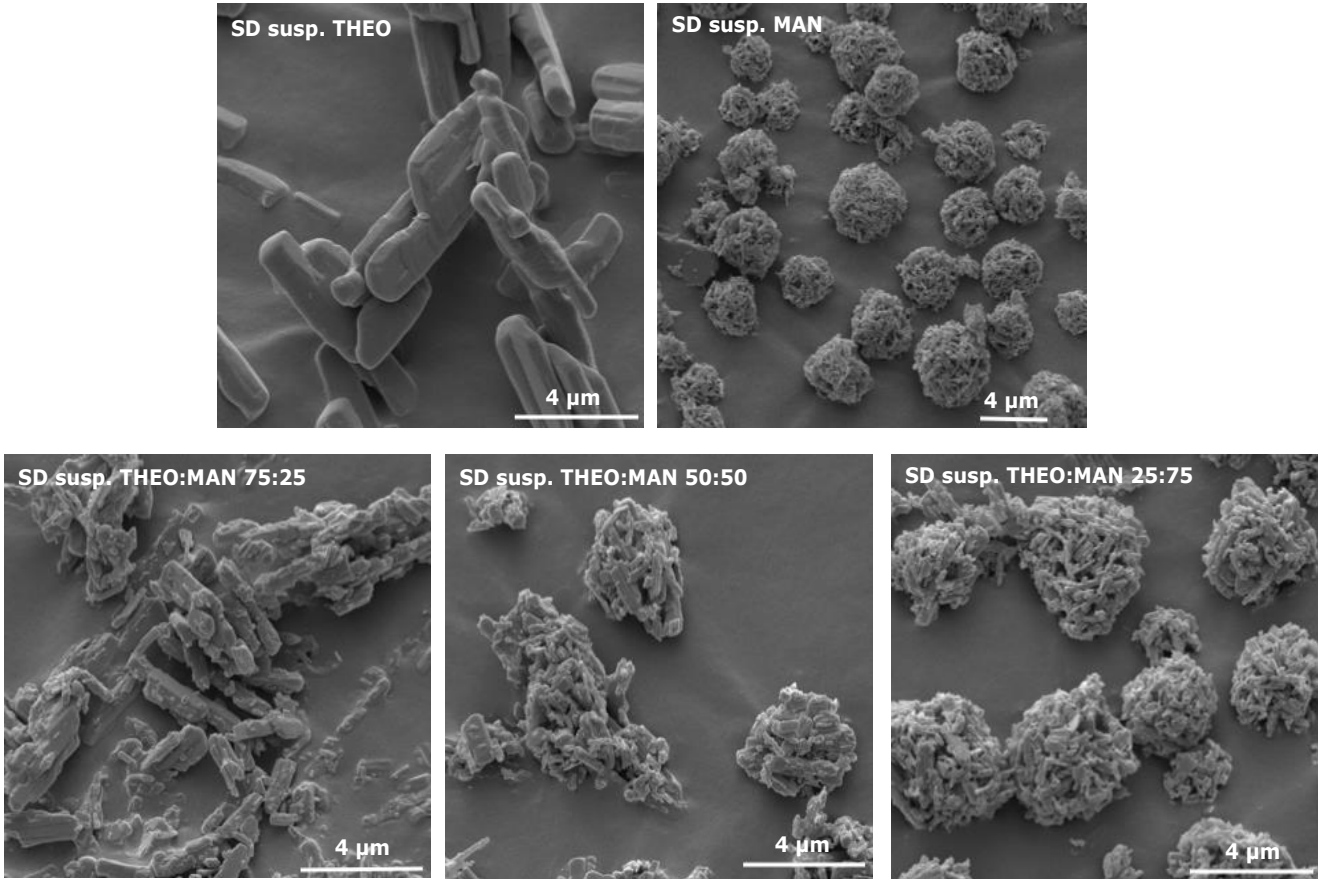

Figure 2. SEM of microcomposite formulations containing theophylline and mannitol wet milled alone and in different mass ratios.

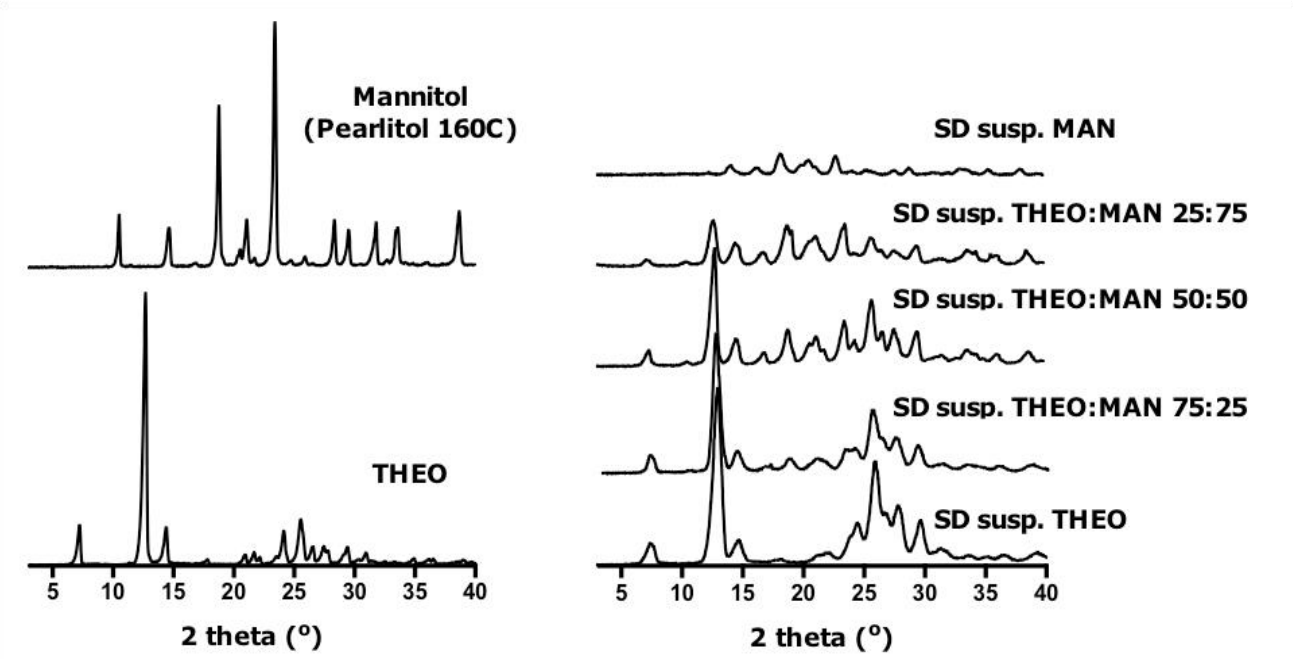

Figure 3. XRPD patterns of starting materials and microcomposite formulations containing different theophylline to mannitol ratios.

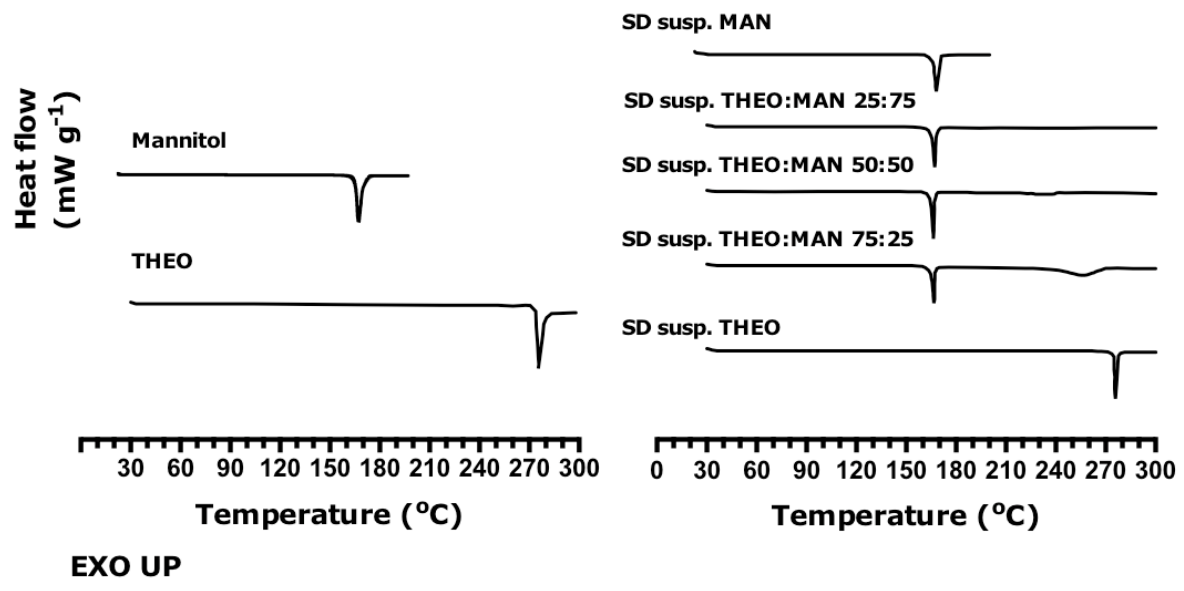

Figure 4. DSC thermograms of starting materials and microcomposite formulations containing different theophylline to mannitol ratios.

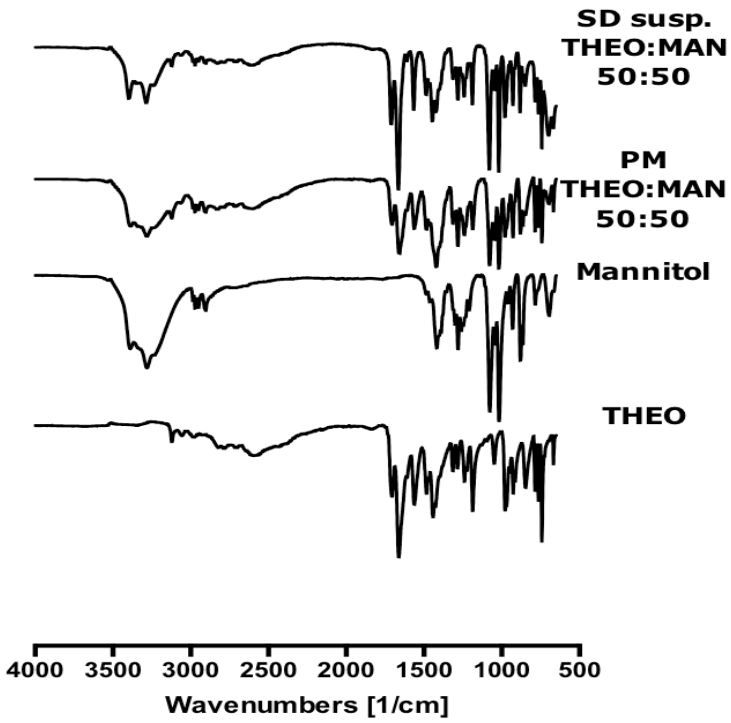

Figure 5. FT-IR spectra of starting materials, physical mixture (PM) of theophylline and mannitol (mass ratio 50:50) and SD susp. THEO:MAN 50:50.

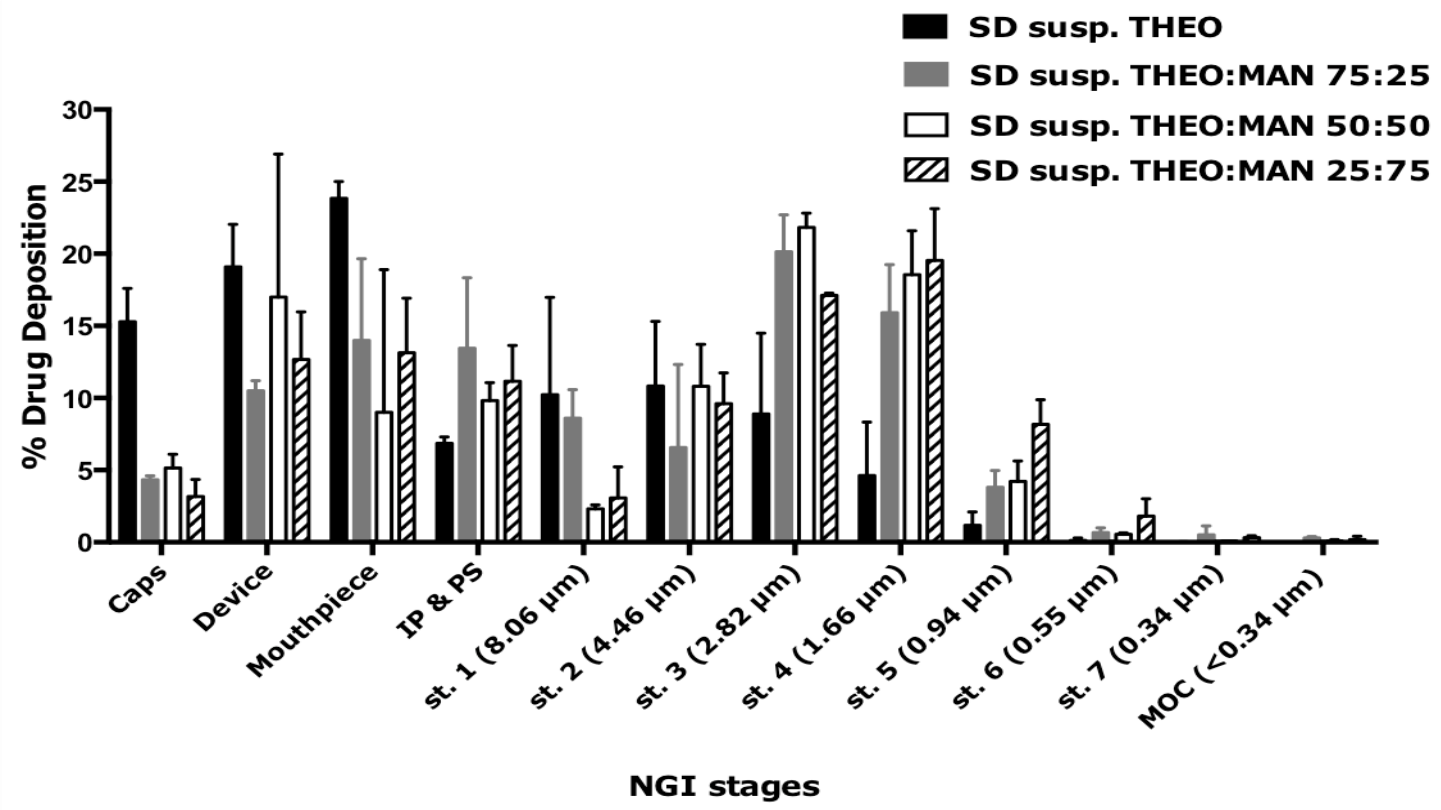

Figure 6. Drug deposition profiles of microcomposites containing different theophylline to mannitol ratios using the Cyclohaler® at 60L min^{-1} (mean + SD, n=3). St.1-St.7 denote stages 1-7 of the NGI, the aerodynamic cut-off diameter of each stage is given in parenthesis.

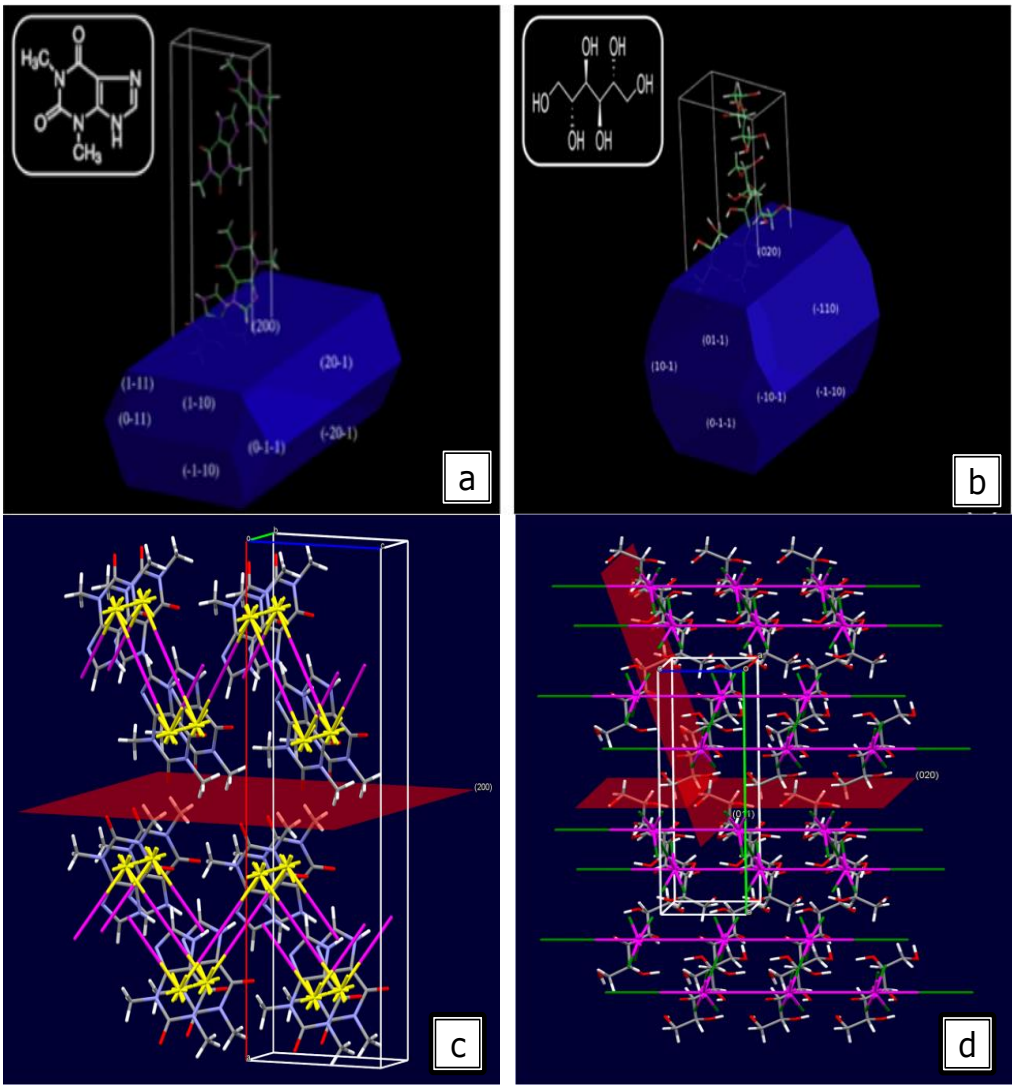

Figure 7. Chemical structures and crystal morphologies of (a) theophylline anhydrous form II and (b) D-mannitol β form. Crystal morphologies are calculated according to the BFDH theory showing the orientation of the unit cell in the bulk crystal. Energy vector diagrams of (c) theophylline form II showing the direction of coulombic and polarisation (pink) and dispersion (yellow) interactions, and of (d) D-mannitol β form, showing the direction of combined stabilising (pink) and destabilising repulsive (green) interactions. Red surfaces indicate the most probable slip planes.

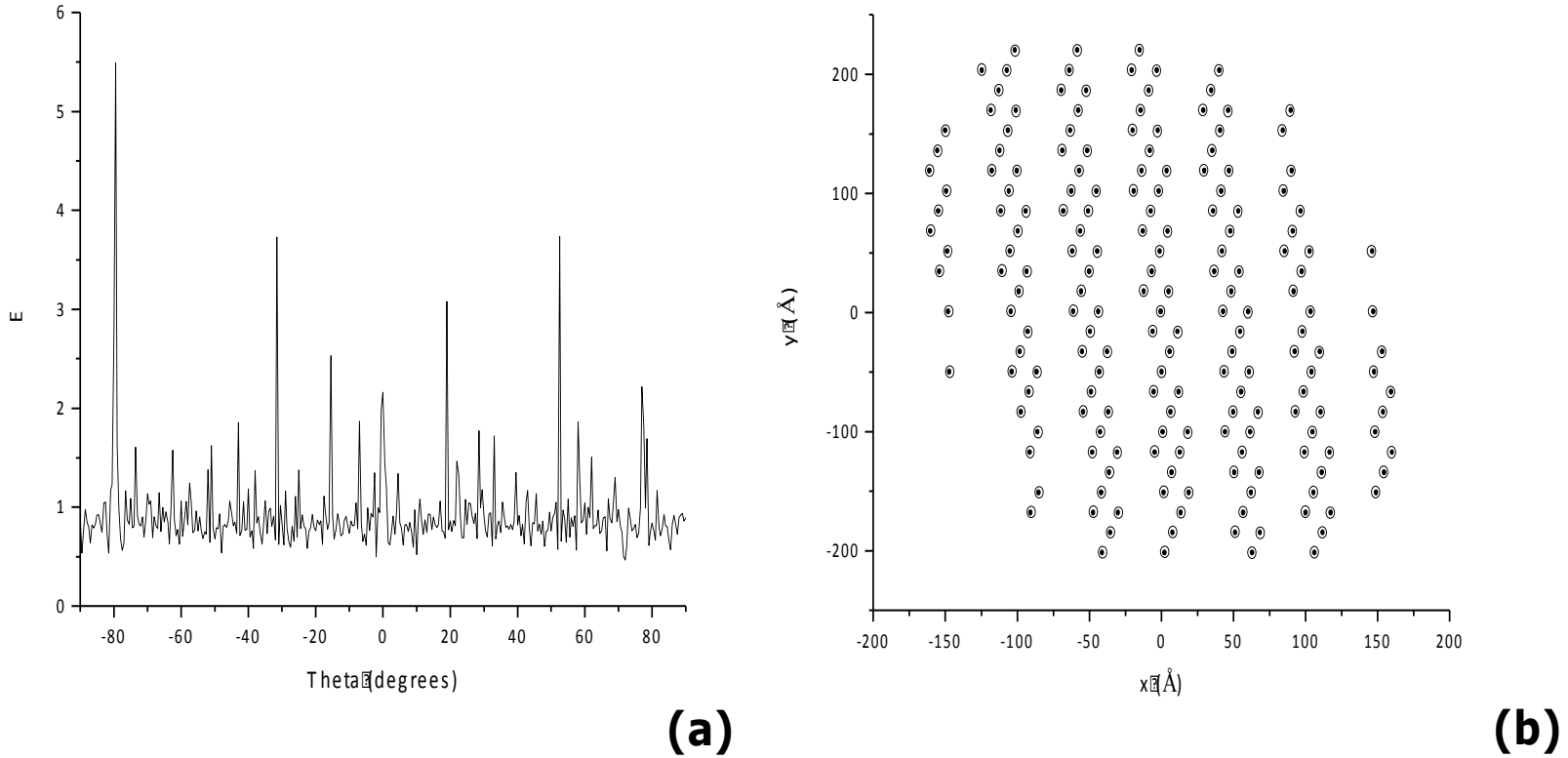

Figure 8. (a) Epitaxy score *vs* rotation angle and (b) Moiré patterns for the geometric matching of theophylline's (100) on mannitol's (011) crystal plane.

1
2